Electrostatic Model Applied to ISS Charged Water Droplet Experiment

Daan Stevenson and Hanspeter Schaub
Dept. Aerospace Engineering Sciences
University of Colorado Boulder
e-mail: daan.stevenson@colorado.edu,
hanspeter.schaub@colorado.edu

Donald R. Pettit
NASA-JSC
Houston, TX

***Abstract*—The electrostatic force can be used to create novel relative motion between charged bodies if it can be isolated from the stronger gravitational and dissipative forces. Recently, Coulomb orbital motion was demonstrated on the International Space Station by releasing charged water droplets in the vicinity of a charged knitting needle. In this investigation, the Multi-Sphere Method, an electrostatic model developed to study active spacecraft position control by Coulomb charging, is used to simulate the complex orbital motion of the droplets. When atmospheric drag is introduced, the simulated motion closely mimics that seen in the video footage of the experiment. The electrostatic force's inverse dependency on separation distance near the center of the needle lends itself to analytic predictions of the radial motion.**

I. Introduction

Scientists have long been interested in electrostatic phenomena, and many experiments have been conducted since the first electrostatic effects were noticed in antiquity. [1] To first order, the force relationship between two charged objects is governed by Coulomb's law, which exhibits the same inverse quadratic position relationship as gravitational attraction. [2] While orbital motion due to gravity is only apparent on a celestial scale, the kiloVolts of electrostatic potential readily generated by the triboelectric effect produces noticeable relative motion within a laboratory setting. Moreover, an extra mode of actuation is possible because charges of equal polarity generate repulsive forces. Today, large electrostatic potentials can be generated with substantial accuracy using high voltage power supplies (HVPS), allowing for repeatable experimentation.

A recent research effort has identified Coulomb charging as a means to control the relative positions of spacecraft in close proximity formations. [3–5] In this scenario, charge control devices such as electron and ion guns are used to raise the absolute potential of the spacecraft to tens of kiloVolts. In high Earth orbit, where the Debye shielding is minimized, the resultant forces can be used for stationkeeping maneuvers, electrostatic tugs, or rendezvous operations. [6–9] In order to simulate the 6DOF relative motion of charged bodies with complex geometries, their electrostatic

interaction must be accurately modeled in a computationally efficient manner. To this end, the Multi-Sphere Method (MSM) has been developed, as discussed further in Section III.

Because of the expensive nature of space flight, terrestrial validation of these concepts is necessary before progressing to on-orbit verification. Various Coulomb testbeds have been created in the Autonomous Vehicle Systems (AVS) Laboratory at the University of Colorado for this purpose. Using HVPSs, conducting shapes are charged up in order to control linear relative position as well as rotation rates and absolute attitudes. [10–12] A common challenge with these experiments is overcoming the friction in the gravitational environment to generate charged relative motion. In 2008, researchers demonstrated electrostatic orbits of spherical conductors on a zero gravity parabolic flight path under NASA's Reduced Gravity Research Program. [13] The analytical stability of such orbits, while considering induced charge effects, is discussed in Reference 14.

During Expedition 30 on the International Space Station (ISS), Flight Engineer Don Pettit demonstrated orbital motion of water droplets about a knitting needle charged by the triboelectric effect. The water droplets were charged to high voltages of opposite polarity using a Van Der Graff generator, and emitted from a syringe in proximity of the needle. Video footage shows the semi-stable orbits of the water droplets about the knitting needle due to their electrostatic interaction. In this paper, those orbits are simulated using the electrostatic models developed for inter-spacecraft charge control. The $1/r$ force relationship that results along the center of the needle lends itself to analytic predictions of the trajectory. Since the orbits are contained along the length of the needle, this research may lend itself to liquid droplet radiator design, whereby waste heat is dissipated from a spacecraft system. [15, 16]

II. ISS Charged Water Droplet Experiment

Knitting needles were flown to the International Space Station (ISS) as crew personal items. The Teflon knitting needle was 215 mm long, 6.4 mm in diameter, with a 17 mm tapered blunt end. The polypropylene knitting needle was 240 mm long, 8 mm in diameter, with a 25 mm tapered blunt end. The knitting needles were mounted by the non-tapered end on an adjustable ball stack arm with Velcro and Kapton tape and placed about 500 mm in front of a background cloth so that droplet trajectories were clearly recorded on video. They were triboelectrically charged by rubbing with crew issued Russian fur boots (fur type unknown). Both knitting needles became negatively charged from this process. One swipe with the fur boots was made between each series of experiments.

Water for creating the drops came from the ISS galley water supply. This water, recovered from urine in the regenerative ISS water system (75% of water in urine recovered) was processed through a distillation apparatus, a series of charcoal filters, particulate filters, de-ionizing resin beds, a catalytic oxidizer, with measured total organic carbon less than 285 ppb (detection limit) and total inorganic carbon of 600 to 650 ppb. Cabin conditions were 19 ± 1 $^{\circ}$C, cabin pressures 745 to 755 mm of Hg, with a composition of 20% oxygen, 79% nitrogen, 0.5% carbon dioxide, and relative humidity of 38 $\pm 3\%$. The level of microgravity was about 1.2×10^{-6}g.

Water was placed in a 25 ml polypropylene syringe fixed with a 12 gauge Teflon cannula. A stainless steel machine screw was driven through the side of the syringe near the exit and was used to charge the water before droplets were ejected from the cannula tip. To charge the water, a belt and rollers Van de Graff generator, made from left over student educational LEGOS and a rubber band, driven by a battery powered drill was used. It was estimated that the Van de Graff generator is capable of creating about 150KV static electric volts from the measured 80 mm length sparks, [17] but the potential imposed on the droplets is estimated to be much lower. Droplets could be made either positive or negatively charged depending on the Van de Graff terminal placed on the syringe machine screw. Typical droplet diameters were 1 to 15 mm in diameter. Negatively charged droplets were forcefully driven away from the charged knitting needle while positively charged droplets with appropriate velocity went into orbit. The droplets were ejected with velocities of a few centimeters per second towards the knitting needle from about 30 to 40 centimeters distance. The initial droplet velocity had both tangent and longitudinal directions to the knitting needle.

Video was recorded with a Canon G1 video camera as HD 1440_1080i format at 29.97 frames per second. Footage was captured from both profile and end views, as can be seen in Figure 1, with the motion of a single droplet transposed on a single image throughout its orbit.

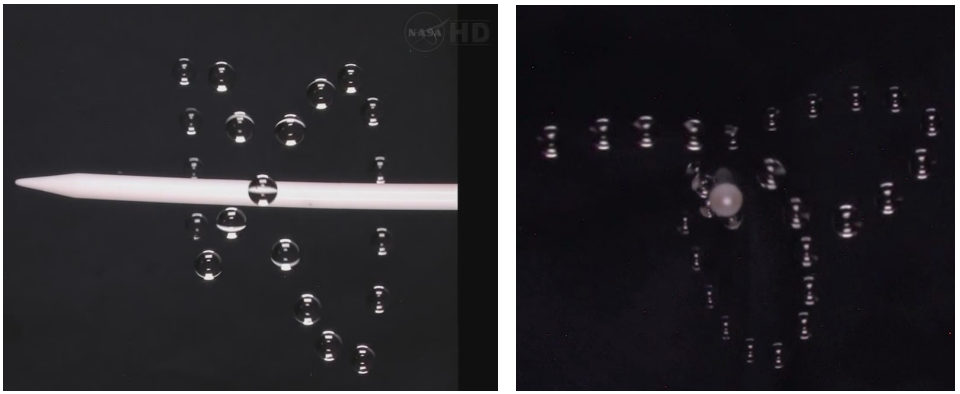

(a) Profile view (b) End view

Fig. 1. Video capture of ISS experiment

III. Multi-Sphere Method

Analytic solutions of Poisson's equation (Eq. 1), which defines electrostatics in 3D space, are rarely possible for complex geometries.

$$\nabla^2\phi(\boldsymbol{x}) = -\frac{\rho(\boldsymbol{x})}{\epsilon_0} \tag{1}$$

Numerous methods exist to approximate electrostatic interactions to various degrees of fidelity. To predict first order electrostatic interaction, charged geometries can be modeled by point charges [18] or by conducting spheres [19]. Since these methods lack the ability to resolve the charge distribution on non-symmetric bodies, they are incapable of predicting electrostatic torques and off-axis forces. Meanwhile, highly accurate numerical solutions are possible by Finite Element Analysis (FEA), but this approach lacks the computational speed necessary for faster-than-realtime 6 Degree of Freedom (6DOF) charged relative motion simulations. The Multi-Sphere Method (MSM), developed for use in spacecraft Coulomb charging research, uses a collection of spheres with fixed sizes and relative positions to model a conducting 3D shape. [20, 21]

Figure 2 depicts satellite A, modeled by n optimally placed spheres, in the vicinity of the simple object B. Both objects are assumed for now to be conducting and reside at voltage levels ϕ_A and ϕ_B. The voltage ϕ_i on a given sphere is a function of the charge q_i on that sphere and the charges on its neighboring spheres. This relation is governed by Eq. (2), [22] where R_i represents the radius of the sphere in question and $\boldsymbol{r}_{i,j} = \boldsymbol{r}_j - \boldsymbol{r}_i$ is the center-to-center distance to each neighbor. The constant $k_c = 8.99 \times 10^9$ Nm^2/C^2 is Coulomb's constant.

$$\phi_i = k_c\frac{q_i}{R_i} + \sum_{j=1,j\neq i}^{m} k_c\frac{q_j}{r_{i,j}} \tag{2}$$

This relationship is most valid when $r_{i,j} \gg R_i$, resulting in a uniform charge distribution on any given sphere. As more spheres are introduced and their size decreases relative to the system size, results become more accurate.

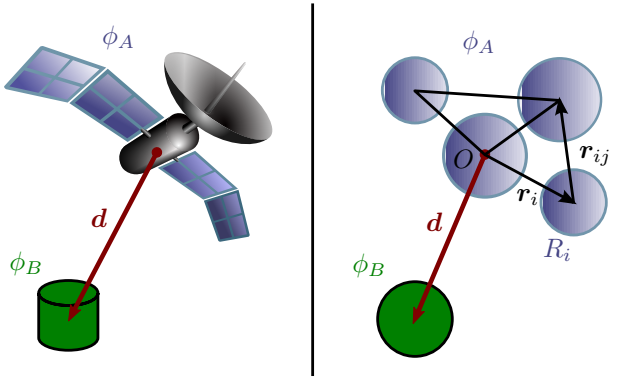

Fig. 2. Conceptual depiction of the Multi-Sphere Method

The linear relations in Eq. (2) can be combined for each of the $m = n + 1$ spheres in the system in Figure 2, resulting in the matrix equation in Eq. (3). Here $\boldsymbol{\phi} = [\phi_A, \phi_A, ..., \phi_A, \phi_B]^T$ and $\boldsymbol{q} = [q_1, q_2, ..., q_n, q_B]^T$ represent matrix collections of the voltages and charges in the entire system.

$$\boldsymbol{\phi} = k_c [C_M]^{-1} \boldsymbol{q} \tag{3}$$

The inverse of the Position Dependent Capacitance (PDC) matrix $[C_M]^{-1}$ is expanded as follows, where $\boldsymbol{r}_{i,B} = \boldsymbol{d} - \boldsymbol{r}_i$:

$$[C_M]^{-1} = \begin{bmatrix} 1/R_1 & 1/r_{1,2} & \cdots & 1/r_{1,n} & 1/r_{1,B} \\ 1/r_{2,1} & 1/R_2 & \ddots & \vdots & \vdots \\ \vdots & \ddots & \ddots & \vdots & \vdots \\ 1/r_{n,1} & \cdots & \cdots & 1/R_n & 1/r_{n,B} \\ 1/r_{B,1} & \cdots & \cdots & 1/r_{B,n} & 1/R_B \end{bmatrix} \tag{4}$$

Next, the array of charges $\boldsymbol{q}$ can be determined by inverting this $n+1$ size symmetric matrix, a fairly straightforward computation. Coulomb's law can then be implemented to calculate the linear force between each charged sphere. Since the location of the spheres within the modeled body are held fixed with respect to each other, their equal and opposite contributions cancel. The total force $\boldsymbol{F}$ and torque $\boldsymbol{L}$ about the origin O on body A due to the object B is given by the following summations:

$$\boldsymbol{F}_A = -\, k_c q_B \sum_{i=1}^{n} \frac{q_i}{{r_{i,B}}^3} \boldsymbol{r}_{i,B} \tag{5}$$

$$\boldsymbol{L}_A = -\, k_c q_B \sum_{i=1}^{n} \frac{q_i}{{r_{i,B}}^3} \boldsymbol{r}_i \times \boldsymbol{r}_{i,B} \tag{6}$$

Because the electrostatic force is conservative and internal to the system, body B will experience a force equal and opposite to the one on A.

The Multi-Sphere Method is similar in its mathematical formulation to simplified versions of the Boundary Element Method (BEM), [23–25] especially when the spheres are populated along the surface of a geometry. [21] However, there is more freedom and efficiency in placement of the elements with the MSM, as spheres can be located within the volume or directly on sharp edges

of a geometry. Moreover, the Multi-Sphere Method (MSM) can be modified to include insulating materials with constant charge.

For spheres within the insulator, a charge is specified rather than a voltage, which are compiled in the vector $\boldsymbol{q}_I$. Combining the mutual capacitance relationship in Eq. 2 for each of the conducting spheres yields

$$\boldsymbol{\phi}_C = k_c[C_C]^{-1}\boldsymbol{q}_C + k_c[C_{C,I}]^{-1}\boldsymbol{q}_I \tag{7}$$

where $[C_{C,I}]^{-1}$ is the mutual capacitance matrix populated with separation distances between the conducting spheres and insulated spheres, with no self capacitance terms. This relationship can be solved for $\boldsymbol{q}_C$ so that the charge on all spheres in the system is known, at which point Eq. 5 and 6 can be equated to determine the force and torque on all bodies in the system. If knowledge of the resulting voltage on the insulating components is desired, it can be determined by:

$$\boldsymbol{\phi}_I = k_c[C_I]^{-1}\boldsymbol{q}_I + k_c[C_{I,C}]^{-1}\boldsymbol{q}_C \tag{8}$$

where $[C_I]^{-1}$ is populated with sphere sizes and relative distances between the insulator spheres, and $[C_{I,C}]^{-1}$ is the transpose of $[C_{C,I}]^{-1}$.

IV. Simulation Parameters

With the Multi-Sphere Method framework in place, the remaining task is to choose an appropriate location and size for all the spheres in the model. In order to model the charged knitting needle, spheres are placed at even distances along the center axis of the needle. This is where the MSM is advantageous over the BEM, which would require elements along the surface of the needle rather than within its volume. The remaining parameter then is to determine the sphere size for a given spacing. This is achieved as in Reference 21, using a nonlinear regression to match the total self capacitance of the needle in space, determined by modeling the geometry in the FEA software Ansoft Maxwell 3D. The capacitance of the MSM body can be computed by summation of the charge q_i on each sphere in the model for a given voltage ϕ:

$$C_{\text{MSM}} = \frac{Q}{\phi} = \frac{\sum_{i=1}^{n} q_i}{\phi} \tag{9}$$

The needle used in the simulation is selected to be 200 mm long with a diameter of 6.5 mm, with the spacing of the spheres set to 6.5 mm. The MSM model consists of 31 spheres, with optimized radius R=4.406 mm. For a conducting geometry, the charge distribution matches the higher order

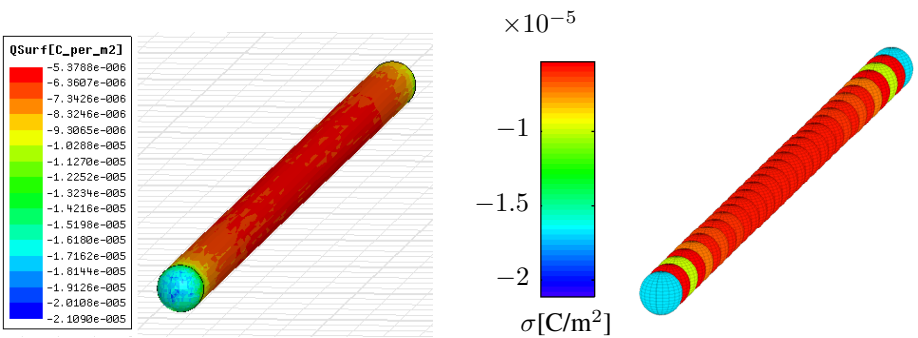

(a) Maxwell 3D (b) MSM

Fig. 3. Charge distribution along knitting needle

solution well, as shown in Figure 3. Since the actual knitting needle is made of insulating material, the simulation maintains a constant charge distribution on all the spheres in the MSM model, such that the entire needle is at an electric potential of -10 kV. The total charge on each sphere is determined from Eq. 7. The orbiting water droplets are of diameter 6.5 mm, and are given a charge equivalent to +20 kV potential in free space.

Integration of the orbital motion of the charged water droplets is performed using a Range-Kutte 45 integrator in Mathworks MATLAB. At each integration step, the MSM algorithm is executed to determine the Coulomb force acting on the droplet. It is also possible to model atmospheric drag within this integration framework, which gradually causes the water droplet orbits to decay and collide with the knitting needle. For an object with cross sectional area A traveling with velocity $\boldsymbol{v}$ through a medium with density ρ, the drag force $\boldsymbol{V}_D$ is given by:

$$\boldsymbol{F}_D = -\frac{1}{2}\rho v C_D A \boldsymbol{v} \tag{10}$$

For a spherical object, the coefficient of drag C_D is dependent on the object's shape and the Reynolds number Re:

$$Re = \frac{\rho v D}{\mu} \tag{11}$$

Here D is the characteristic linear dimension, or the diameter of the water droplet, and μ is the dynamic viscosity of the medium. For a spherical particle, Reference 26 gives the following empirical coefficient of drag:

$$C_D = (24/Re)(1 + 0.1935 Re^{0.6305}) \quad \text{for } 20 < Re \leq 260 \tag{12}$$

The Reynolds number stays within this regime for all the simulations considered here. The International Space Station is pressurized to the same pressure as at sea level on Earth, resulting in a density $\rho = 1.225$ kg/m^3, and viscosity $\mu = 1.81 \times 10^{-5}$ kg/m/s.

V. Analytic Analysis of Orbits

The nature of the MSM algorithm, with its matrix inversion and Coulomb force summation, is very nonlinear. However, for the water droplet orbiting the charged needle, a fairly symmetric force field exists. This can be seen in Figure 4, which shows the force vector at various positions surrounding the needle.

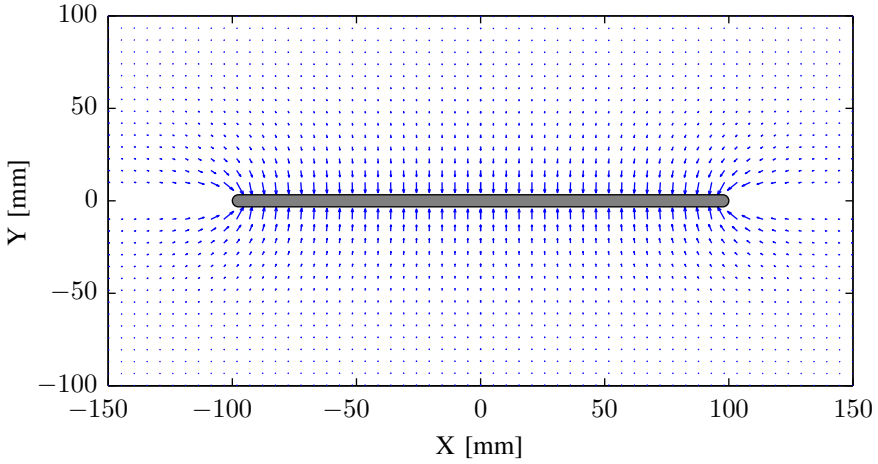

Fig. 4. Force field of a droplet around the needle

If the parallel and perpendicular components of the force are separated, as in Figure 5, it becomes clear that the vertical (radial) force stays relatively constant along the length of the needle. In fact, the radial force varies inversely with radial distance r from the needle. It can be fit with great accuracy to the function

$$F_r = -\frac{a}{r} \tag{13}$$

where $a = 1.6879 \times 10^{-5}$ and the R-squared value of the fit is 0.9986. The inverse force relationship is to be expected from an infinite line charge source. This fit slightly overpredicts the forces as the separation distance increases, which is to be expected because the knitting needle is of finite length. The R-squared value stays as high as 0.95 out to within 10 mm from the end of the needle. If the droplet stays within these bounds, then this analytic relation can be used to predict radial motion in the orbits, which is separable from the horizontal motion. This is likely if the parallel velocity is sufficiently small so that the horizontal restoring force pushes the droplet back toward the center of the needle before the radial force drops off due to the edge effects.

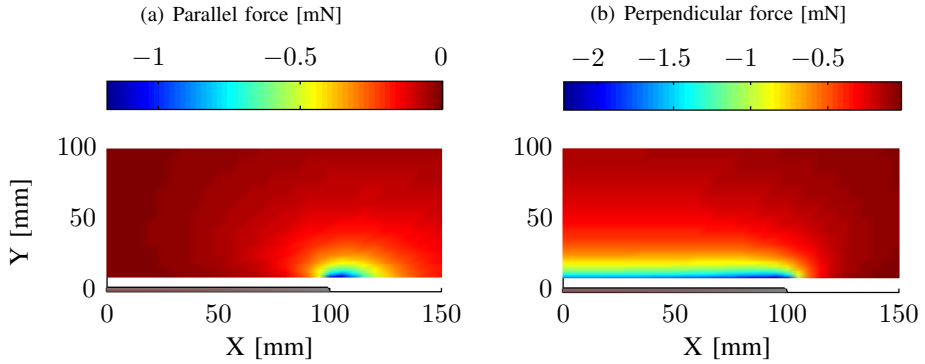

Fig. 5. Horizontal and vertical forces acting on droplet

If the radial force is separable from the horizontal force, we can treat the radial motion as if it were restricted to a plane that lies perpendicular to the length of the needle. This reduces the problem to the central force scenario, with potential

$$U(r) = -\int F_r \mathrm{d}r = a \ln r \tag{14}$$

Because the problem is spherically symmetric, the angular momentum $l = mr^2\dot{\theta}$ is known to be conserved, where m is the mass of the droplet and $\dot{\theta}$ is the angular rate of the motion about the needle. [27,28] Since the electrostatic force is conservative, total mechanical energy E (kinetic and potential) is also conserved:

$$E = T + U = \frac{1}{2}mv^2 + U(r) \tag{15}$$

$$= \frac{1}{2}m(\dot{r}^2 + r^2\dot{\theta}^2) + U(r) \tag{16}$$

$$= \frac{m\dot{r}^2}{2} + \frac{l^2}{2mr^2} + U(r) \tag{17}$$

For the moment, it is assumed that the droplet experiences no dissipative forces. The relation above can be solved for $\dot{r}$:

$$\dot{r} = \pm\sqrt{\frac{2}{m}(E - U) - \frac{l^2}{m^2 r^2}} \tag{18}$$

Setting this relation equal to zero allows one to solve for r_{min} and r_{max}:

$$E - a \ln r - \frac{l^2}{2mr^2} = 0 \tag{19}$$

Due to the logarithmic potential function, this solution must be obtained numerically. Equation 17 can be manipulated to determine the angular position as a function of the radius:

$$\mathrm{d}\theta = \frac{\mathrm{d}\theta}{\mathrm{d}t}\frac{\mathrm{d}t}{\mathrm{d}r}\mathrm{d}r = \frac{\dot{\theta}}{\dot{r}}\mathrm{d}r = \frac{l}{mr^2\dot{r}}\mathrm{d}r \tag{20}$$

which can be integrated to determine the precession of the orbit between the radial extremes:

$$\Delta\theta = 2\int_{r_{\text{min}}}^{r_{\text{max}}} \frac{(l/r^2)\mathrm{d}r}{\sqrt{2m\left(E - U - \frac{l^2}{2mr^2}\right)}} \tag{21}$$

A circular orbit will occur at a given separation distance if the radial force is exactly equal to the required centripetal acceleration.

$$F_r = mr\dot{\theta}^2 \tag{22}$$

$$\dot{\theta} = \sqrt{\frac{a}{m}}\frac{1}{r_0} \tag{23}$$

Figure 6 shows an end view of three orbits with different initial conditions, one producing a circular orbit, and the others with less initial energy. These types of orbits are clearly identifiable in the end view video footage, as seen in Figure 1(b). Wolfram Mathmatica is used to numerically solve Eq. (19) for the minimum and maximum radii, and integrate Eq. (21) for the expected precession of each orbit. The predicted results match the orbits in the simulation extremely well, even when the droplet has an initial velocity component along the length of the needle. If the droplet is given an initial velocity greater than circular, the orbits exhibit similari behavior, but r_0 becomes the lower bound r_{min}.

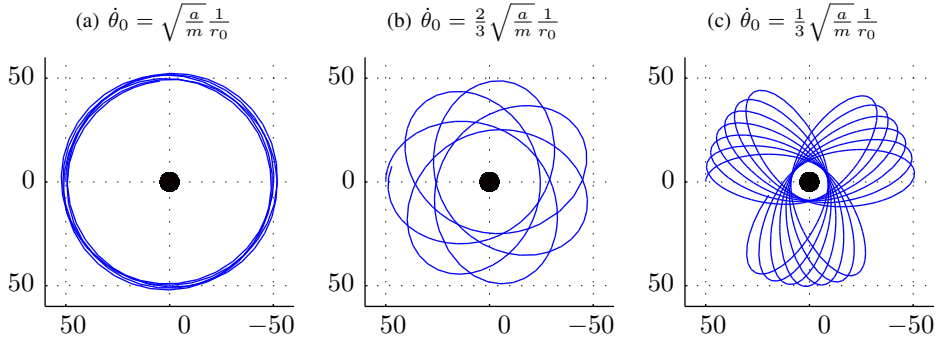

Fig. 6. Planar orbits with various initial velocities [Scale in mm]

Because the potential $U(r)$ grows unbounded for large separation distances, it is theoretically impossible for the droplet to reach escape the orbit of the needle. In the simulation and within the experiment, however, the droplets often exhibit hyperbolic orbits. This is because with a finite length needle, the forces drop off slightly quicker than $1/r$ at large separation distances. Due to the finite needle length, as r increases the needle acts more like a point charge with a $1/r^2$ force field.

TABLE I
PREDICTED ORBITAL PARAMETERS

$\dot{\theta}_0$	$r_{\min}$ [mm]	$r_{\max}$ [mm]	$\Delta\theta$ [deg]
$\sqrt{\frac{a}{m}\frac{1}{r_0}}$ (circular)	50	50	N.A.
$\frac{2}{3}\sqrt{\frac{a}{m}\frac{1}{r_0}}$	24.22	50	251.4
$\frac{1}{3}\sqrt{\frac{a}{m}\frac{1}{r_0}}$	8.80	50	240.5

VI. SIMULATION RESULTS

The full MSM simulation with drag forces implemented is executed for various initial velocity conditions. The results are shown in Figure 7. The initial droplet position is at $r_0 = 50$ mm, in the center of the needle. For most of the simulations, the motion is contained within 10 mm of the end of the needle, where the radial forces drop off predictably and the radial motion is predictable as in the planar cases in the previous section. Due to the atmospheric drag acting on the droplet, however, all orbits gradually decay and in some cases the simulation is terminated by collision with the needle. The motion closely matches the various orbits visible in the video footage of the ISS demonstration.

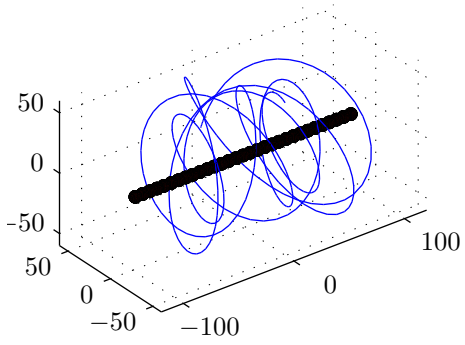

(a) $v_{\parallel 0}$ =150 mm/s, $v_{\perp 0}$ =400 mm/s

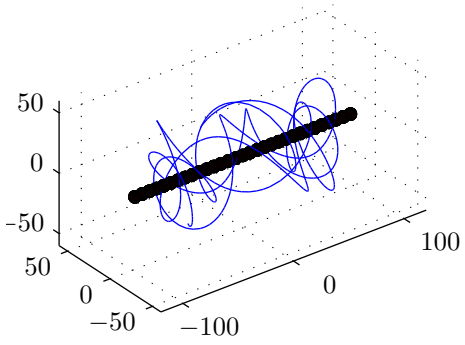

(b) $v_{\parallel 0}$ =200 mm/s, $v_{\perp 0}$ =200 mm/s

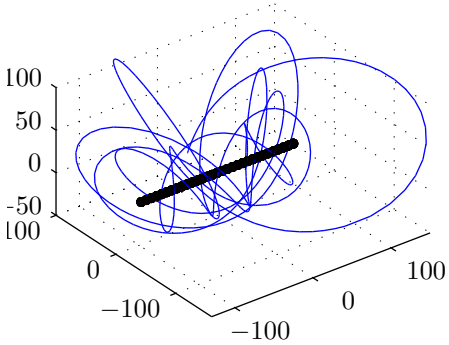

(c) $v_{\parallel 0}$ =200 mm/s, $v_{\perp 0}$ =500 mm/s

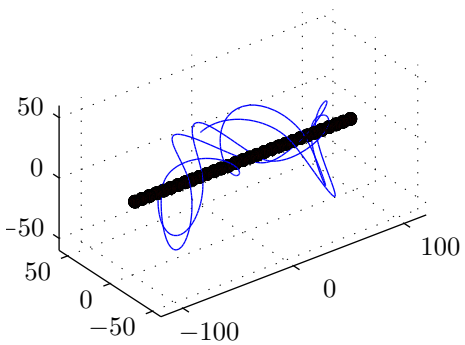

(d) $v_{\parallel 0}$ =200 mm/s, $v_{\perp 0}$ =100 mm/s

Fig. 7. Simulation of orbital motion including drag for various initial conditions [Scale in mm]

VII. Conclusion

In this investigation, a electrostatic orbits of water droplets about a charged knitting needle in a microgravity environment are analyzed. An electrostatic model developed for spacecraft charging applications uses a collection of spheres to determine the charge distribution and relative forces and torques on various geometries. By modifying this model to capture the behavior of insulating material, it can be used to simulation the motion of the particles. Mapping out the force field acting on the droplets around the needle suggests that the force varies with the inverse of the radial distance along the majority of the needle, and horizontal forces ensure that the particle generally remains within this regime. Because of this inverse force relationship, several analytic predictions are made regarding the apogee and perigee, as well as the precession angle of the orbits. When atmospheric drag is included in the simulation, the 3D motion that results accurately matches the orbits seen in video recordings of the ISS experiment.

References

[1] G.W. Francis and O.D. Jefimenko. *Electrostatic Experiments: An Encyclopedia of Early Electrostatic Experiments, Demonstrations, Devices, and Apparatus*. Electret Scientific, 2005.

[2] Islam I Hussein and Hanspeter Schaub. Invariant shape solutions of the spinning three craft coulomb tether problem. *Celestial Mechanics and Dynamical Astronomy*, 96(2):137–157, 2006.

[3] Lyon B. King, Gordon G. Parker, Satwik Deshmukh, and Jer-Hong Chong. Spacecraft formation-flying using inter-vehicle coulomb forces. Technical report, NASA/NIAC, January 2002.

[4] Lyon B. King, Gordon G. Parker, Satwik Deshmukh, and Jer-Hong Chong. Study of interspacecraft coulomb forces and implications for formation flying. *AIAA Journal of Propulsion and Power*, 19(3):497–505, May–June 2003.

[5] Hanspeter Schaub, Gordon G. Parker, and Lyon B. King. Challenges and prospect of coulomb formations. *Journal of the Astronautical Sciences*, 52(1–2):169–193, Jan.–June 2004.

[6] Erik Hogan and Hanspeter Schaub. Collinear invariant shapes for three-craft coulomb formations. *Acta Astronautica*, 12:78–89, March–April 2012.

[7] Hanspeter Schaub and Daniel F. Moorer. Geosynchronous large debris reorbiter: Challenges and prospects. In *AAS Kyle T. Alfriend Astrodynamics Symposium*, Monterey, CA, May 17–19 2010. Paper No. AAS 10-311.

[8] Erik Hogan and Hanspeter Schaub. Relative motion control for two-spacecraft electrostatic orbit corrections. In *AAS/AIAA Spaceflight Mechanics Meeting*, Girdwood, Alaska, July 31 – August 4 2011. Paper AAS 11–466.

[9] Trevor Bennett, Daan Stevenson, Erik Hogan, Lauren McManus, and Hanspeter Schaub. Prospects and challenges of touchless debris despinning using electrostatics. In *3rd European Workshop on Space Debris Modeling and Remediation*, CNES, Paris, June 16–18 2014. Paper #P8.

[10] Carl Seubert. One-dimensional spacecraft formation flight testbed for terrestrial charged relative motion experiments. 2011.

[11] Daan Stevenson and Hanspeter Schaub. Terrestrial testbed for remote coulomb spacecraft rotation control. *International Journal of Space Science and Engineering*, 2(1):96–112, 2014.

[12] Daan Stevenson and Hanspeter Schaub. Advances in experimental verification of remote spacecraft attitude control by coulomb charging. In *GNC 2014: 9th International ESA Conference on Guidance, Navigation and Control Systems*, Porto, Portugal, June 2–6 2014.

[13] Shubho Banerjee, Kevin Andring, Desmond Campbell, John Janeski, Daniel Keedy, Sean Quinn, and Brent Hoffmeister. Orbital motion of electrically charged spheres in microgravity. *The Physics Teacher*, 46(8):460–464, 2008.

[14] Shubho Banerjee, Bradford Taylor, and Anand Banerjee. On the stability of electrostatic orbits. *arXiv preprint arXiv:0808.3993*, 2008.

[15] AT Mattick and A Hertzberg. Liquid droplet radiators for heat rejection in space. *Journal of Energy*, 5(6):387–393, 1981.

[16] AT Mattick and A Hertzberg. Liquid droplet radiator performance studies. *Acta Astronautica*, 12(7):591–598, 1985.

[17] Ezinwa O Elele, Yueyang Shen, Donald R Pettit, and Boris Khusid. Detection of a dynamic cone-shaped meniscus on the surface of fluids in electric fields. *Physical review letters*, 114(5):054501, 2015.

[18] Shuquan Wang. Shape control of charged spacecraft cluster with two or three nodes. 2010.

[19] Carl R. Seubert and Hanspeter Schaub. Electrostatic force model for terrestrial experiments on the coulomb testbed. In *61st International Astronautical Congress*, Prague, CZ, Sept. 2010. International Astronautical Federation. Paper IAC-10.C1.1.9.
[20] Daan Stevenson and Hanspeter Schaub. Multi-sphere method for modeling spacecraft electrostatic forces and torques. *Advances in Space Research*, 2012.
[21] Daan Stevenson and Hanspeter Schaub. Optimization of sphere population for electrostatic multi sphere model. In *12th Spacecraft Charging Technology Conference, Kitakyushu, Japan*, 2012.
[22] W. R. Smythe. *Static and Dynamic Electricity*. McGraw–Hill, 3rd edition, 1968.
[23] C.A. Brebbia. *The boundary element method for engineers*. Pentech Press, 1978.
[24] Walton C. Gibson. *The Method of Moments in Electromagnetics*. Chapman and Hall/CRC, 1st edition, 2007.
[25] V.A. Davis and M.J. Mandell. Plasma interactions with spacecraft, vol. ii. Technical report, AFRL, April 2011. NASCAP-2K Scientific Documentation for Version 4.1.
[26] Roland Clift, John R Grace, and Martin E Weber. *Bubbles, drops, and particles*. Courier Corporation, 2005.
[27] Jerry B Marion. *Classical dynamics of particles and systems*. Academic Press, 2013.
[28] Herbert Goldstein. *Classical mechanics*. Pearson Education India, 1957.